ANNALS of Faculty Engineering Hunedoara – International Journal of Engineering

Tome XII [2014] – Fascicule 4 [November]
ISSN: 1584-2673 [CD-Rom, online]

a free-access multidisciplinary publication of the Faculty of Engineering Hunedoara

[1,2.] F. O. ARAMIDE, [1,2.] K. K. ALANEME, [3.] P.A. OLUBAMBI, [1,2.] J.O. BORODE

EFFECTS OF 0.2Y-9.8ZrO_2 ADDITION ON THE MECHANICAL PROPERTIES AND PHASE DEVELOPMENT OF SINTERED CERAMIC PRODUCED FROM IPETUMODU CLAY

[1.] Department of Metallurgical and Materials Engineering, Federal University of Technology, P.M.B. 704, Akure, NIGERIA
[2.] African Materials Science and Engineering Network, (AMSEN) a Subsidiary of Regional Initiative for Science Education (RISE)
[3.] Applied Microscopy and Triboelectrochemical Research Laboratory, Department of Chemical and Metallurgical Engineering, Tshwane University of Technology, Pretoria, SOUTH AFRICA

Abstract: The effects of the addition of yttria stabilized zirconia and sintering temperatures on the phases developed and the mechanical properties of sintered ceramic produced from Ipetumodu clay was investigated. The clay of known mineralogical compositions was thoroughly blended with 2% (vol) yttria, 8% (vol) zirconia. From this and the raw clay standard samples were prepared, fired at 1200°C and 1300°C. The sintered samples were then characterized for the developed phases using x-ray diffractometry analysis, microstructural morphology using ultra-high resolution field emission scanning electron microscope (UHR-FEGSEM) and various mechanical properties. It was observed that primary mullite and sillimanite were developed in the samples produced. The samples produced solely from the raw clay could not withstand 1300°C due to stress induced by the transformation from one silica phase to another. This phase transformation also adversely affected the mechanical properties of the sintered raw clay. The additive improved on the mechanical properties of the samples by the consumption of the silica phases to form zircon phase in addition with the other phases and the excess zirconia. It was concluded that the sample fired at 1300°C have the optimum mechanical properties.
Keywords: yttria stabilized zirconia; sintering temperatures; phases developed; clay; sintered ceramic

1. INTRODUCTION

The word ceramics is a broad name which is applicable in many products. They possess good corrosion resistance and ability to preserve their properties at a high temperature up to 1200°C.

Other useful properties that make the ceramic attractive for engineering applications include excellent high-temperature strength and creep resistance, good thermal and chemical stability, low thermal-expansion coefficient, low true density, wear resistance and good dielectric properties [1-6]. Recently, many researchers have focused their investigations on how to improve the properties of ceramics for various applications. Zum Gahr [7], demonstrated that modification of the microstructure could reduce the friction and the wear of alumina. Likewise in 1996, he showed that reducing the grain size of alumina and zirconia will significantly decrease the wear [8].

Furthermore Dong *et al* [9], specified the effect of both single additives (MgO, SiO_2, Fe_2O_3 and ZrO_2) and compound additives on the mechanical and thermal properties of aluminum titanate ceramics, and finally pointed out that the compound additives of MgO and Fe_2O_3 have an excellent improvement on the stability of aluminum titanate. Jiang *et al* [10], also demonstrated that the role of additives can be rationalized in terms of promotion of sintering process, formation of new phases and influence on lattice constant of aluminum titanate ceramics.

Ebadzadeh and Ghasemi [11], observed that the addition of TiO_2 to mullite-ZrO_2 composites prepared from different alumina sources results into change of reaction sintering, densification and microstructure which can alternately alter the formation temperature and retention of t-ZrO_2

phase in these composites. Moya *et al*. [12] demonstrated that the microstructure of mullite-zirconia and alumina- zirconia composites can be modified by additives like CaO and MgO.

Ipetumodu is a town in Osun State, in the southwestern part of Nigeria. The size of the town is 64 km² (25 sq mi). The town is the headquarters of Ife North local government Area. It is located at an elevation of 227 meters above sea level and its population amounts to 164,172. Its coordinates are 7°31'0" N and 4°27'0" E.

Various researchers have investigated the properties of this clay deposit for industrial applications [13-16]. But there is no record of the investigation of the effects of the concerned additives on the mechanical properties and phase development of the sintered ceramic produced from clay sourced from the deposit.

2. MATERIALS AND METHODS

2.1. Materials

Clay Samples used in this work were sourced from Ipetumodu, Osun State in the south western part of Nigeria. High purity oxides such as zirconia and yttria were supplied by F.J. BODMANN & CO, L.L.C. (The Thermal Spray Materials and Technologies Source). Oakmere Business Park, 2072 Sussex Street, Harvey, LA 70058.

2.2. Raw Clay Preparation

The clay samples were first soaked in water for three days to dissolve the deleterious materials in them and at the same time to form slurry. The slurries were then sieved to remove deleterious materials and other foreign substances. The sieved slurries were then allowed to settle down for three days after which the clear floating water was decanted. The dispersed fine clays in water (clay slurries) were then poured into plaster of Paris (P.O.P) moulds and left undisturbed for three days in order to allow the remaining water present to drain out completely. The resulting plastic clay masses were sun dried and subsequently dried in a laboratory oven at 110°C for 24 hours. The resulting dried clay samples were crushed and milled in a Rawwley Sussex grinder to an average particle size of 300µm.

2.3. Chemical and Mineralogical Composition of Raw Clay Samples

The compounds present in the samples were determined by x-ray fluorescence (XRF). The results obtained are presented in Table 1. The mineralogical phases present in the samples were also determined using x-ray diffractometry (XRD). The phases present are reported in Figure 1 and Table 2. The chemical composition of the clay samples were determined using atomic absorption spectroscopy (AAS). The results obtained are presented in Table 3. Ultra-high resolution field emission scanning electron microscope (UHR-FEGSEM) equipped with energy dispersive spectroscopy (EDS) was used to examine the microstructure of the clay samples. The observed microstructures are presented in Figures 2, 3, 4 and 5.

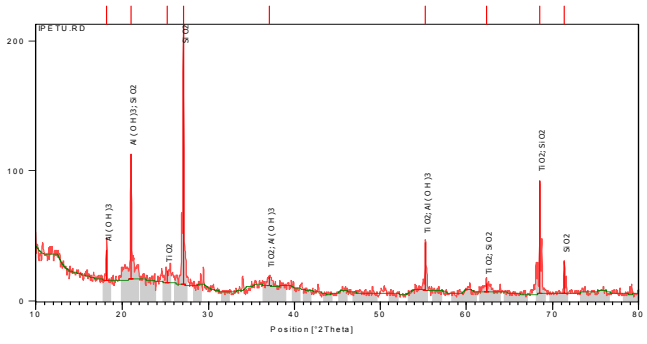

Figure 1: X-Ray Diffraction Pattern (Phase Analysis) of Ipetumodu Clay Sample

Table 1: XRF Semi-quantitative analysis of the elements of raw clay samples (weight %)

Phases	Amount (%)
Al_2O_3	25.03
SiO_2	57.482
Fe_2O_3	9.226
K_2O	1.259
MgO	0.91
CaO	0.763
Na_2O	0.372
TiO_2	1.512
Zr	0.103
Total	97.1

Table 2: XRD Result of the Raw Clay Samples Showing the Quantity of Different Phases Present

Phases	Weight (%)
Kaolinite	23.74
Microcline	26.12
Muscovite/Illite	15.02
Plagioclase/ Albite	11.28
Quartz	23.84

Table 3. Chemical Composition of Raw Clay Samples (%)

Samples	SiO_2	Al_2O_3	Fe_2O_3	TiO_2	CaO	MgO	Na_2O	K_2O	LOI
Raw Clay	54.82	25.90	1.44	2.08	0.12	0.15	0.2	1.57	11.64

Table 4. XRD Result of the Sintered Ceramic Samples RT1, FT1 and FT2 Showing the Quantity of Different Phases Present

Samples	Quartz	Hematite	Mullite	Sillimanite	Pseudobrookite	Iron(III) Niobium Oxide (1/1/4)	Rutile	Aluminium Niobate(V)	Zircon	m-ZrO_2	Cristobalite
RT1	14.1	9.26	42.51	6.63	4.63	0	0.54	0	0	0	22.3
FT1	8.16	4.72	7.37	16.07	1.26	0.42	0.45	1.91	4.12	42	13.52
FT2	1.96	3.96	10.97	18.38	1.12	0.78	1.39	2.53	23.19	28.8	6.92

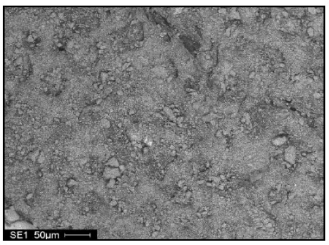

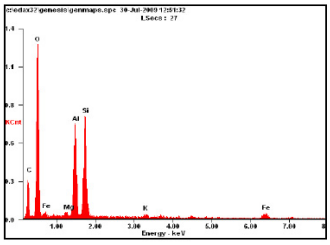

Element	Weight (%)
C	15.06
O	46.354
Mg	00.688
Al	12.626
Si	17.434
K	01.08
Fe	07.324

Figure 2. Typical SEM/EDS micrographs of Raw Clay Sample showing the morphology of the mineral and its chemical composition

2.4. Preliminary Testing of Sintered Raw Clay

The clay sample from Ipetumodu was first milled in a high energy planetary ball mill at 300 rev/min for 4 hour to obtain average particle size of 75µm. Standard dimensions test samples were produced from the milled clay; for phase analysis and SEM/EDS analysis and mechanical properties by compacting in a stainless steel mold using a load of 750 MPa. The green compact were then sintered (fired) at 1200°C and 1300°C (T1 and T2 respectively) held for an hour, in an electric furnace. The samples were designated as "R" The sample sintered at 1200°C were subjected to various tests such as determination of the phases developed in the sample due to sintering using XRD and bulk density, apparent porosity, cold crushing strength modulus of elasticity, and absorbed energy. The results obtained are shown in Tables 4 and 5 for XRD and mechanical properties respectively.

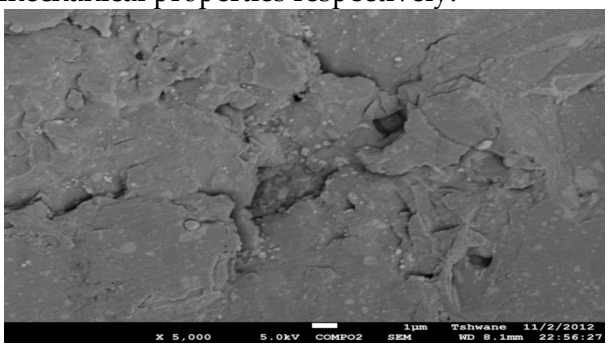

(a)

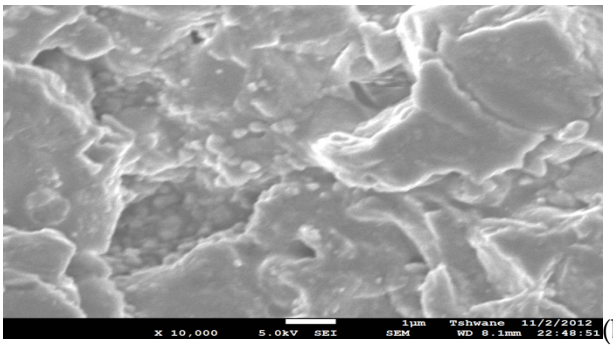

(b)

Figure 3. Typical SEM micrographs of Sample RT1 showing its morphology and cracks (a) Back Scattered Image and (b) Secondary Electron Image

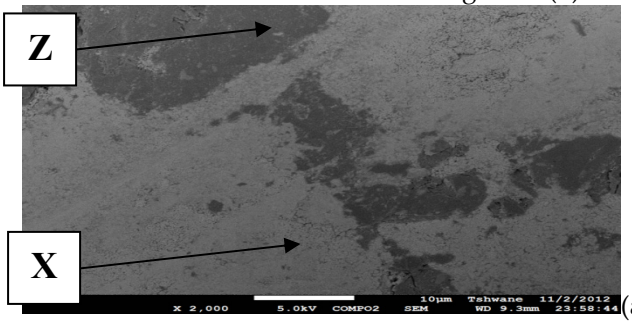

(a)

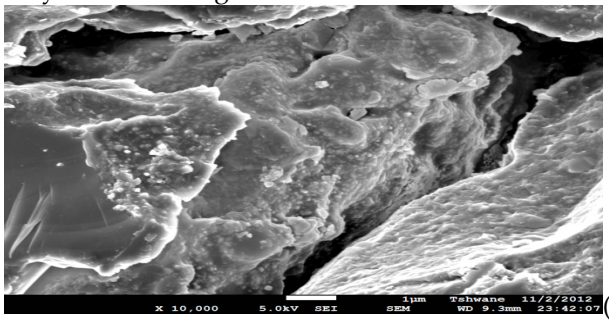

(b)

Figure 4. Typical SEM micrographs of Sample FT1 showing its morphology (a) Back Scattered Image and (b) Secondary Electron Image X= Phase with ZrO_2, while Z=phases of sintered clay

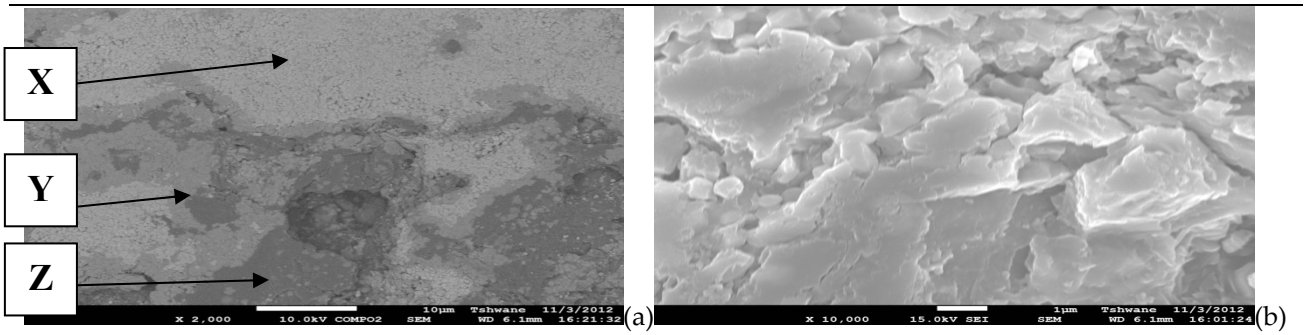

Figure 5. Typical SEM micrographs (Back Scattered Image) of Sample FT2 showing its morphology (a) Back Scattered Image and (b) Secondary Electron Image. X= Phase with ZrO_2, Y= Zircon phase, while Z=phases of sintered clay

2.5. Powder Blending

The mass percent of the composition below was computed using Equations (1) and (2) using the densities in Table M2 and the individual powders volume fraction in each composition. The powders were weighed per batch of 50.00 g on a sensitive electronic weighing balance to five (5) decimal places. The individual (batch) composition was thoroughly mixed in a Turbula Mixer for 18 hours at a speed of 72 rev/min. The compositions of the blended samples were shown in Table M1.

Table M1. The Compositions of Samples produced from blended powders used for the Experimental Investigations

Designation	Raw Clay (Vol. %)	Zirconia (ZrO_2) (Vol. %)	Yttria (Y_2O_3) (Vol. %)
F	90	9.8	0.2

Table M2. Densities of Various Components used

Oxide/Clay	Clay[a]	ZrO_2[b]	Y_2O_3[b]
Density (g/cm^3)	1.20	5.68	5.01

If

$$M_t = V_{cl}\varrho_{cl} + V_{Zr}\varrho_{zr} + V_Y\varrho_Y \quad (1)$$

where V_{cl}, V_{Zr}, and V_Y are respectively the volume fraction of clay, ZrO_2 and Y_2O_3, ϱ_{cl}, ϱ_{Zr} and ϱ_Y are respectively the volume fraction of clay, ZrO_2 and Y_2O_3, and M_t is the total mass contribution of all the components. And if M is the mass of each batch, then the mass contribution of each component could be calculated from:

$$Mc = \frac{V_{c\varrho c}\, xM}{M_t} \quad (2)$$

Mc is the mass contribution of a component in a batch (clay or ZrO_2 or Y_2O_3), Vc, ϱ_c the respective volume fraction and density of the component.

The resulting homogenous powder mixtures were compacted uniaxially into standard sample dimensions for cold crushing strength, bulk density, porosity measurements and thermal shock resistance. The samples were compressed uniaxially using 750 Mpa compaction load inside a standard stainless steel die. The resulting green compacts were fired at 1200°C (for FT1) and 1300°C (for FT2) in an electric furnace. The sintered samples were then characterized for various mechanical properties as described below:

[a]Determined in the laboratory

[b]Provided by the supplier

2.6. Testing

2.6.1. Apparent Porosity

Test samples from each of the ceramic composites were dried for 12 hours at 110°C. The dry weight of each fired sample was taken and recorded as D. Each sample was immersed in water for 6 hrs to soak and weighed while been suspended in air. The weight was recorded as W. Finally, the specimen was weighed when immersed in water. This was recorded as S. The apparent porosity was then calculated from the expression:

$$p = \frac{(W - D)}{(W - S)} x100\% \quad (3)$$

The results obtained are presented in Table 5.

Table 5: Mechanical Properties of Samples RT1, FT1 and FT2

Samples	Thermal Shock Resistance (cycles)	Apparent Porosity (%)	Bulk Density (g/cm^3)	Cold Crushing Strength (N/mm^2)	Absorbed Energy (J)	Young's Modulus E (N/mm^2)
RT1	+30	22.70	1.95	1833.3	0.4320	21363
FT1	+30	17.50	1.87	4409.00	1.2919	55208
FT2	+30	15.40	2.06	8447.00	4.1753	64994

2.6.2. Cold Compression Strength, Modulus of Elasticity and Absorbed Energy

Cold compression strength test is to determine the compression strength to failure of each sample, an indication of its probable performance under load. The standard ceramic samples were dried in an oven at a temperature of 110°C, allowed to cool. The cold compression strength tests were performed on INSTRON 1195 at a fixed crosshead speed of 10mm min^{-1}. Samples were prepared according to ASTM C133-97 (ASTM C133-97, 2003) and cold crushing strength, modulus of elasticity and absorbed energy of standard and conditioned samples were calculated from the equation:

$$CCS = \frac{LoadToFracture}{SurfaceAreaOfSample} \quad (4)$$

The results obtained are presented in Table 5.

2.6.3. Bulk Density

The test specimens were dried at 110°C for 12 hours to ensure total water loss. Their dry weights were measured and recorded. They were allowed to cool and then immersed in a beaker of water. Bubbles were observed as the pores in the specimens were filled with water. Their soaked weights were measured and recorded. They were then suspended in a beaker one after the other using a sling and their respective suspended weights were measured and recorded. Bulk densities of the samples were calculated using the formula below:

$$\text{bulk density} = \frac{D}{(W - S)} \quad (5)$$

where: D = Weight of dried specimen, S = Weight of dried specimen suspended in water, and W = Weight of soaked specimen suspended in air. The results of this are presented in Table 5.

2.6.4. Thermal Shock Resistance

Each sample of the clay/saw dust blend was placed in an electrically heated furnace to attain the test temperature of 1000°C for over 3 hours. Each sample was then with- drawn from the furnace and held for 10 minutes. The procedure was repeated until an appearance of a crack was visible. The number of cycles necessary to cause a crack was recorded for each of the samples and taken as a measure of its thermal shock resistance.

2.7. Analysis

2.7.1. Qualitative and Quantitative XRD

The samples were prepared for XRD analysis using a back loading preparation method. They were analysed using a PANalytical X'Pert Pro powder diffractometer with X'Celerator detector and variable divergence- and receiving slits with Fe filtered Co-Kα radiation. The phases were identified using X'Pert Highscore plus software. Graphical representations of the qualitative result follow below. The relative phase amounts (weights %) were estimated using the Rietveld method (Autoquan Program). Amorphous phases, if present were not taken into consideration in the quantification. The results obtained are presented in Figure 2 and Tables 2 and 4.

2.7.2. Scanning Electron Microscopy

Morphology and microanalysis of the clay and composite samples were determined using ultra-high resolution field emission scanning electron microscope (UHR-FEGSEM) equipped with energy dispersive spectroscopy (EDS). The pulverized clay samples/sintered ceramic composite samples were previously gold coated. The samples were studied using ultra-high resolution field emission scanning electron microscope (UHR-FEGSEM) equipped with energy dispersive spectroscopy (EDS). Particle images were obtained with a secondary electron detector. The

SEM/EDS micrographs of the powder clay and the various sintered ceramic samples are shown in Figures 2 to 5.

2.7.3. Chemical Analysis

(a) X-Ray Fluorescence (XRF) - The major elements were determined by X-ray fluorescence with an ARL® 9800 XP spectrometer. The pulverized clay samples were mixed with lithium tetraborate for chemical analysis. The ignition loss was measured by calcinations at 1000°C. The XRF result is shown in Table 1.

(b) Atomic Absorption Spectroscopy (AAS) - The chemical analysis of the clay samples was also carried out using atomic absorption spectrophotometry (AAS) method with Spectra AA 220 FS Machine. The percentage compositions of the various constituents were then recorded in Table 3.

3. RESULTS AND DISCUSSION

3.1. Phase Development and Mechanical Properties of the Sintered Raw Ipetumodu Clay

Tables 4 and 5 shows respectively the phases developed in the samples RT1/1, FT1/1 and FT2/1 and the mechanical properties of samples RT1/1, FT1/1 and FT2/1. Figure 3 shows the micrographs of the sample RT1/1.

3.1.1. Phase Development in the Sintered Raw Ipetumodu Clay

From Table 4 the phases developed in the ceramic sample produced from the raw Ipetumodu clay and sintered at 1200°C (RT1/1) are clearly shown. Comparing this with the XRD results shown in Table 2 the total silica (quartz) in the clay is 23.84%, but in the fired sample, the total silica (quartz and cristobalite) is 36.4%. The excess/extra silica comes from the mullitization process. Moreover, it is observed that the sample RT1/1 contains mullite and sillimanite as listed above, comparing these with Table 2, it is observed that the clay sample contains 23.73% kaolinite and above 37% feldspar.

When kaolinite is fired, the following transformations occur in its structure: The dehydration of kaolinite completes by ~150°C, followed by dehydoxylation at ~420-660°C and its structural breakdown occurs in the temperature range ~800-900°C, depending upon the particle size and amount and type of the impurities present. The kaolinite in the Ipetumodu clay (Table 2) containing 23.84% quartz, 15.02% muscovite/illite (and about 37% feldspars) dehydroxylates to metakaolinite at ~420-660°C depending on the type and amount of impurities present [17, 18, 19] via

$$Si_2Al_2O_5(OH)_4 \xrightarrow{420\text{-}660C} Al_2O_3{*}2SiO_2 + 2H_2O \quad (6)$$

which involves the combination of two OH groups to form H_2O and oxygen which remains incorporated in metakolin. At about 900°C, metakaolinite decomposes to amorphous SiO_2 and γ-Al_2O_3–type spinel via

$$Al_2O_3.2SiO_2 \xrightarrow{900C} \gamma\text{-}Al_2O_3{+}2SiO_2 \quad (7)$$

γ-Al_2O_3–type spinel and SiO_2 recrystallize into mullite at temperatures above 1100°C via

$$3\gamma\text{-}Al_2O_3{+}2SiO_2 \xrightarrow{>1100C} 3Al_2O_3.2SiO_2 \quad (8)$$

Srikrishna, et al [20], reported the formation of a single phase (with composition close to mullite) and excess SiO_2 at 900°C. Thus the formation of mullite begins at temperatures >900°C and the process continues till 1000°C

From the Table 4, it is observed that the amount of mullite developed in the RT1 is 42.51%. This is not unconnected with the presence of hematite and rutile in the raw clay on one hand and the presence of feldspar on the other hand.

Different authors have demonstrated that mullitization can be increased by catalytic ions such as Fe^{3+} and Ti^{4+} [21, 22]. These metallic ions help in mullite formation by replacing the Al^{3+} ions in the glass structure during firing. The presence of small amounts of Fe^{3+} and Ti^{4+} in kaolin modifies the chemical composition of the ceramic bodies and therefore the sintering behaviour which in the case of porcelain is characterized by mullitization. It can be observed from Table 3 that the sintered sample RT1 contains 4.63% pseudobrookite and 0.54% rutile which are oxides of iron and titanium. The phenomenon of mullitization is also influenced by the grade of feldspar which particularly

affects the formation of secondary mullite. The quality of feldspar is determined by the amount of orthoclase and albite. Nowadays, mixed feldspars are considered suitable fluxing agents for porcelain manufacture since they develop a very viscous liquid phase that embeds the new forming crystals and part of the residual crystals present in the microstructure, enhancing the densification process [23, 24]. However, from the SEM images of the sample RT1, the mullite needles could not be seen (Figure 2). The mullite in the RT1 as seen the Table 3 is the primary mullite as explained in the following paragraphs. Mullite formed from kaolin clay alone is termed primary mullite whereas that formed from reaction with an alkali flux is termed secondary. In vitrified triaxial porcelains of the clay–feldspar–flint composition, mullite crystals of two or three distinctive morphologies have been reported [25-31].

Apart from the shape, the crystals can also be differentiated by their size and aspect ratio [31], and by the chemical composition that changes from the nonstoichiometric 2:1 of primary mullite to the stoichiometric 3:2 of seconday mullite [29] on heating to temperatures higher than 1400°C in triaxial compositions.

Primary mullite of composition close to 2:1, forms only from clay relicts of mostly kaolinite ($Al_2O_3.2SiO_2.2H_2O$) at 1100°–1150°C as small crystals of <0.5μm or <0.1μm in size. Scaly crystals forming at lower temperatures are the direct product of clay minerals, and have a characteristic cuboidal shape as observed under the TEM. Comer [32], found that primary mullite crystals in vitrified kaolin, although of the characteristic needle shape, were less than 1 μm long. From the crystal size alone, TEM observations suggested that they were similar to primary mullite (of scaly appearance) and secondary mullite (of granular shape) [25, 27-34].

Furthermore, mullite crystals produced in clay–feldspar relicts are secondary mullite with several morphologies, such as the granular, cuboidal [29, 30, 31, 35], acicular, or needlelike [25, 35]. Iqbal et al. [29, 30] further defined secondary mullite in the fine clay, feldspar, and quartz matrix based on the aspect ratio [30, 31]. They were observed from both model and commercial [31] triaxial porcelains vitrified at temperatures above 1400°C.

3.1.2. Mechanical Properties of the Sintered Raw Ipetumodu Clay

It is observed from Table 5 that the sintering temperature has a direct impact of the thermal shock resistance of the raw clay. The higher the sintering temperature the better the thermal shock resistance of the sample. This is expected, as the samples were initially prepared/fired at higher temperature than the temperature at which the thermal shock resistance tests were carried out. From the same table, the cold crushing strength (CCS), Young's Modulus (E), absorbed energy, apparent porosity and bulk density of the sample prepared from the raw sample (RT1) alone were observed to be 1833.3 N/mm^2, 21363 N/mm^2 and 0.432 J, 22.70% and 1.95 g/cm^3 respectively.

3.2. Phase Development in the Sintered Samples FT1 and FT2

From Table 4 the phase development in the samples FT1 and FT2 are clearly seen. At T1 (1200°C), it is observed that the sample contains 8.16% quartz, 4.72% hematite, 7.37% mullite, 16.07% sillimanite, 1.26% pseudobrookite, 0.42% $FeNbO_4$, 0.45% rutile, 1.91% $AlNbO_4$, 4.12% zircon, 42% m-ZrO_2, and 13.52% cristobalite. Increasing the sintering temperature to T2 (1300°C), the phases observed in the samples are; 1.96% quartz (reduction), 3.96% hematite (reduction), 10.97% mullite (increase), 18.38% sillimanite (increase), 1.12% pseudobrookite (reduction), 0.78% $FeNbO_4$ (increase), 1.39% rutile (increase), 2.53% $AlNbO_4$ (increase), 23.19% zircon (increase), 28.8% m-ZrO_2 (reduction), and 6.92% cristobalite (reduction).

It is observed that there were reductions in the amount of quartz, cristobalite phases (which are silica) and m-ZrO_2, in the sample at 1300°C, FT2 (when compared with the sample at 1200°C, FT1). Conversely, it is observed that there was an increase in the amount of zircon phase in the sample FT2 when compared with the amount in FT1 (compare Figures 4 and 5). This is because as the sintering temperature is increased from 1200°C to 1300°C the silica and the zirconia acquired enough energy for the following solid state reaction:

$$ZrO_{2(s)} + SiO_{2(s)} \rightarrow ZrSiO_{4(s)} \quad (9)$$

This accounts for the reduction in the quartz, cristobalite and m-ZrO_2 phases and the increase in the zircon phase as stated above. The changes observed in the other phases could be explained as due to the contribution of the product of the solid state reaction of equation (9) in the weight (%) of the sample. From the Table 3, the total weight percent consumed as a result of the solid state reaction is 26% but the weight percent increase observed in the zircon is just 19.07%. There is a deficit of 6.93% which will lead to change in the percentage contents of other phases.

3.3. Mechanical Properties of the Sintered Samples FT1 and FT2

Table 5 shows the mechanical properties of the sintered samples. It is observed that the apparent porosity of the sample at 1200°C (FT1), is 17.50%. As the sintering temperature is increased to 1300°C (FT2), the apparent porosity reduced to 15.40%. This could be explained that increase in the sintering temperature allowed for more densification to take place thereby allowing more pores to be filled by the liquid phase present at the concerned temperature thereby reducing the porosity of the sample. It is also observed that the bulk density of the sample at 1200°C (FT1), is 1.87 g/cm^3, as the sintering temperature is increased to 1300°C (FT2), the apparent porosity reduced to 2.06 g/cm^3. This behavior is also due to the reduced porosity of the sample as explained above which lead to increase in the amount of matter in the sample per unit volume. Furthermore, it is observed at 1200°C (FT1) that the cold crushing strength (CCS), absorbed energy and the Young's modulus are respectively 4409 N/mm^2, 1.2919 J and 55208 N/mm^2. Moreover, as the sintering temperature is increased to 1300°C (FT2), the cold crushing strength (CCS) increased to 8447 N/mm^2, the absorbed energy also increased to 4.1753 J similarly, the Young's modulus also increased to 64994 N/mm^2. The reason for this is that the bulk density of the sample increased with the sintering temperature (consequent to reduction in the apparent porosity of the samples with increased sintering temperature), which means that there more matter in the sample to bear the applied load [13, 19, 36]. Similarly, from Figures 4(b) and 5(b), it is clearly observed that the cracks observed in sample FT1 (Figure 4a) due to the phase transformation from one silica phase to another, were completely sealed off by the zircon phase in sample FT2 (Figure 5b). This is also responsible for the improved mechanical property of FT2 when compared with FT1. The thermal shock resistances of the samples were observed to be more than 30 cycles. This is due to the fact that the samples were earlier sintered at higher temperature than the temperature at which the test was carried out.

3.4. Comparison of the Mechanical Properties of Sintered Sample RT1/1 with FT1/1 and FT2/1

Comparing the mechanical properties of sample RT1/1 with those of the FT1/1 and FT2/1, it was observed that the addition of 10% volume of yttria stabilized zirconia improved the mechanical properties of the sample. It is noted from Table 4 that sample RT1/1 contains 14.1% quartz and 22.3% cristobalite, FT1/1 contains 8.16% quartz and 13.52% cristobalite while FT2/1 contains 1.96% quartz and 6.92% cristobalite. These phases have marked differences in their thermal expansion coefficients and the glass matrix. During cooling from the sintering temperature to room temperature, the marked differences in thermal expansion results in internal residual stresses which adversely affects the strength of the sample [37]. Sample RT1/1 has the highest amount of quartz and cristobalite, followed by FT1/1 while the least amount of the mentioned phases were observed in FT2/1. This explained why the sample RT1/1 has very low strength, when compared with the other two samples and why the strength of FT1/1 is about half of that of FT2/1. This is also the reason why the sample RT2/1 cracked/failed and could not be further work upon.

4. CONCLUSION

It can be concluded that:

- ✓ Due to phase transformation of the silica content of the Ipetumodu clay from one silica phase to another during sintering, the mechanical properties of the ceramic produced from it sintered at 1200°C is very low and could not withstand a firing temperature of 1300°C;

- ✓ Addition of 2% (vol) yttria, and 8% (vol) zirconia resulted into depletion of the silica phases, formation of zircon phase and excess zirconia in addition with other phases improved on the mechanical properties of the samples fired at 1200°C and 1300°C
- ✓ The optimum mechanical properties is obtained in the samples fired at 1300°C

Acknowledgements

The authors wish to acknowledge the following organizations for their support. They are Regional Initiative in Science Education (RISE), Science Initiative Group (SIG) and African Materials Science and Engineering Network (AMSEN).

Reference

[1.] Aksay, I. A; Dabbs, D. M and Sarikaya, M. Mullite for structural, electronic, and optical application. *J. Am. Ceram. Soc.*, 1991, 74(10), 2343-2358.
[2.] Kanzaki, S; Tabata, H; Kumazawa, T. and Ohta, S. Sintering and mechanical properties of stoichmiometric mullite. *J. Am. Ceram. Soc.*, 1985, 68(1), C6.
[3.] Dokko, P. C; Pack, J. A. and Mazdiyasni, K. S. High temperature mechanical of mullite under compression. *J. Am. Ceram. Soc.*, 1977, **60**(3-4), 150-155.
[4.] Schneider, H. and Eberhand, E., Thermal expansion of mullite. *J. Am. Ceram. Soc.*, 1990, 73(7), 2073-2076.
[5.] R. F. Dovis and J. A. Posk, Diffusion and reaction studies in the system Al_2O_3-SiO_2. *J. Am. Ceram. Soc., 1972*, **5**(10), 525-531.
[6.] Aksay, I. A. and Pask, J. A. Stable and metastable equilibria in the system SiO_2-Al_2O_3. *J. Am. Ceram. Soc., 1975*, 58(11-12), 507-512.
[7.] Zum Gahr, K.-H. Effect of grain size on friction and sliding wear of oxide ceramics, Wear 162–164 (1993) 269–279.
[8.] Zum Gahr, K.-H. Modeling and microstructural modification of alumina ceramic for improved tribological properties, Wear 200 (1996) 215–224.
[9.] Dong Xiu-zhen, Wang Yi-ming, Li Yue. Additives' effect on aluminium titanate ceramics [J]. China Ceramics, 2008, **44**(1): 7–10.
[10.] Jiang Lan, Chen Xiao-yan, Han Guo-ming, Meng Yu Effect of additives on properties of aluminium titanate ceramics, Trans. Nonferous Met. Soc. China, 2011, **21**, 1574-1579
[11.] Ebadzadeh, T. and Ghasemi, E. Effect of TiO_2 addition on the stability of t-ZrO_2 in mullite-ZrO_2 composites prepared from various starting materials, *Ceramics International*, 2002, **28**, 447–450.
[12.] Moya, J.S; Miranzo, P. and Osendi, M.I. Influence of additives on the microstructural development of mullite-ZrO_2 and alumina-ZrO_2, *Materials Science and Engineering*, 1989, **AI09**, 139-145.
[13.] Aramide, F.O. Effect of Firing Temperature on Mechanical Properties of Fired Masonry Bricks Produced from Ipetumodu Clay, Leonardo Journal of Sciences, 2012, Issue 21, 70-82.
[14.] Durotoye, B; Ige, A. and Awojide, P.O. Small scale mining of clay deposit at Ipetumodu, near Ile- Ife, Oyo State, *Journal of Mining and Geology*, 1988, **24**(l&2), p. 65-69.
[15.] Ibitoye, S.A and Afonja, A.A. Adaptation of Ipetumodu potter's clay to foundry use: 1. Moulding properties of as mined and silica mixed potter's clay, *Ife Journal of Technology*, 1997, **7**(1), p. 17-22.
[16.] Ibitoye, S.A and Afonja, A.A. Adaptation of Ipetumodu potter's clay to foundry use: 2. Development of potter's clay bound synthetic moulding sand, *Ife Journal of Technology*, 1997, **7**(1), p. 39-45.
[17.] Qiu, G; Jiang, T; Li, G; Fan, X. and Huang, Z. Activation and removal of silicon in Kaolinite by thermochemical process, Scan. J. Metallurgy, **33**, (2004), 121-128.
[18.] Aramide, F.O. Production and Characterization of Porous Insulating Fired Bricks from Ifon Clay with Varied Sawdust Admixture. *Journal of Minerals and Materials Characterization and Engineering*, 2012, **11**, 970-975.
[19.] Aramide, F.O. and Seidu, S.O. Production of Refractory Lining for Diesel Fired Rotary Furnace, from Locally Sourced Kaolin and Potter's Clay, *Journal of Minerals and Materials Characterization and Engineering*, 2013, **1**, 75-79 doi:10.4236/jmmce.2013.13014 Published Online May 2013 (http://www.scirp.org/journal/jmmce)
[20.] Srikrishna, K; Thomas, G; Martinez, R; Corral, M.P; Aza, S.D. and Moya, J.S. Kaolinite-Mullite reaction series: A TEM study, J. Mater. Sci., **25**, (1990), 607-612.
[21.] Kausik, D; Sukhen, D. and Swapan, K. D. Effect of substitution of fly ash for quartz in Triaxial kaolin–quartz–feldspar system, *J. Eur. Ceram. Soc.* **24**, (2004), 3169–3175.
[22.] Omani, H; Hamidouche, M; Madjoubi, M.A; Louci, K; Bouaouadja, N. and Etude, de la Transformation de trois nuances de kaolin en fonction de la temperature, Silicate Industriel, **65**(11–12), 2000, 119–124.
[23.] Chatterjee, A; Chitwadgi, S; Kulkarni, M. and Kaviraj, A.K. Effect of sodium and Potassium feldspar ratio on the phase development and microstructure of fired porcelain tiles, *Indian Ceram.* 2001, **44** (1), 11–14.
[24.] Esposito, L; Salem, A; Tucci, A; Gualtieri, A. and Jazayeri, S.H. The use of nepheline-syenite in a body mix for porcelain stoneware tiles, Ceram. Int. 2005, **31**(2), 233–240.
[25.] Carty, W.M. and Senapati, U. Porcelain - Raw Materials, Processing, Phase Evolution, and Mechanical Behavior, *J. Am. Ceram. Soc*. 1998, **81**(1), 3-20.
[26.] Lundin, S.T. "Electron Microscopy of Whiteware Bodies," *Trans. Int. Ceram*. Congr., **4**, (1954), 383–390.
[27.] Schuller, K.H. "Reactions between Mullite and Glassy Phase in Porcelains," *Trans. Br. Ceram. Soc.*, **63** (2), 1964, 102–17.
[28.] Lundin, S.T. "Microstructure of Porcelain," Natl. Bur. Stand. (U.S.) Misc. Publ., **257**, (1964), 93–106.
[29.] Iqbal, Y. and Lee, W.E. "Fired Porcelain Microstructures Revisited," *J. Am. Ceram. Soc*., 1999, **82** (12), 3384–90.

[30.] Iqbal, Y. and Lee, W.E. "Microstructural Evolution in Triaxial Porcelain," *J. Am. Ceram. Soc.*, 2000, **83**(12), 3121–3127.
[31.] Iqbal, Y. and Lee, W.E. "Influence of Mixing on Mullite Formation in Porcelain," *J. Eur. Ceram. Soc.*, 2001, **21**(14), 2583–86.
[32.] Comer, J.J. "Electron Microscopy of Mullite Development in Fired Kaolinite," *J. Am. Ceram. Soc.*, 1960, **43**(7), 378–384.
[33.] Castelein, O; Guinebretière, R.; Bonnet, J.P. and Blanchart, P. Shape, size and composition of mullite nanocrystal from a rapidly sintered kaolin, *J. Eur. Ceram. Soc.*, (2001), **21**, 2369-2376.
[34.] Schuller, K.H. and Kromer, H. (1976) "Primary Mullite as a Pseudomorph after Kaolinite", 533–538, in Proceedings of the *International Clay Conference* (Mexico City, 1975). Edited by S. W. Bailey. Applied Publishing, Wilmette, IL.
[35.] Chen, Y.F; Wang, M.C. and Hon, M.H. "Secondary Mullite Formation in Kaolin– Al_2O_3 Ceramics," *J. Mater. Res.*, 2004, **19**(3), 806–814.
[36.] Norton, F. H., (1968) Refractories, 4th Edition, *McGraw-Hill*, New York.
[37.] Akwilapo, D. L. and Wiik, K. Ceramic Properties of Pugu Kaolin Clays. Part 2: Effect of Phase Composition on Flexural Strength, *Bull. Chem. Soc. Ethiop*. 2004, **18**(1), 7-16.

ANNALS of Faculty Engineering Hunedoara – International Journal of Engineering